The Journal of Immunology

Mycobacterium tuberculosis Infects Dendritic Cells with High Frequency and Impairs Their Function In Vivo

Andrea J. Wolf, Beth Linas, Giraldina J. Trevejo-Nuñez, Eleanor Kincaid, Toshiki Tamura, Kiyoshi Takatsu and Joel D. Ernst

J Immunol 2007; 179:2509-2519; ;
doi: 10.4049/jimmunol.179.4.2509
http://www.jimmunol.org/content/179/4/2509

The Journal of Immunology is published twice each month by
The American Association of Immunologists, Inc.,
1451 Rockville Pike, Suite 650, Rockville, MD 20852

Print ISSN: 0022-1767 Online ISSN: 1550-6606.

Mycobacterium tuberculosis Infects Dendritic Cells with High Frequency and Impairs Their Function In Vivo[1]

Andrea J. Wolf,*† Beth Linas,* Giraldina J. Trevejo-Nuñez,* Eleanor Kincaid,*† Toshiki Tamura,‡ Kiyoshi Takatsu,[2§] and Joel D. Ernst[2*†¶‖]

Mycobacterium tuberculosis **(Mtb) is thought to reside in macrophages, although infected dendritic cells (DCs) have been observed. Thus, although cellular associations have been made, global characterization of the cells harboring Mtb is lacking. We have performed temporal and quantitative characterization of the cells harboring Mtb following aerosol infection of mice by using GFP-expressing bacteria and flow cytometry. We discovered that Mtb infects phagocytic cells of diverse phenotypes, that the predominant infected cell populations change with time, and that myeloid DCs are the major cell population infected with Mtb in the lungs and lymph nodes. We also found that the bacteria in the lung-draining lymph node are transported there from the lungs by a CCL19/21-dependent mechanism and that the transport of bacteria to the lymph node is a transient phenomenon despite chronic infection. In addition, we found that the lymph node cell subsets that are most efficacious in stimulating Mtb-specific, TCR-transgenic $CD4^+$ T lymphocytes are not infected with the bacteria and are scarce or absent from the lungs of infected mice. Finally, we found that the lung cell populations that are infected with Mtb at high frequency are relatively ineffective at stimulating Ag-specific $CD4^+$ T lymphocytes, and we have obtained evidence that live Mtb can inhibit MHC class II Ag presentation without a decrease in the surface expression of MHC class II. These results indicate that Mtb targets DC migration and Ag presentation in vivo to promote persistent infection.** ***The Journal of Immunology,*** **2007, 179: 2509–2519.**

Mycobacterium tuberculosis (Mtb)[3] is an exceptionally successful pathogen, which indicates that it is particularly successful at evading immune responses. Humans and experimental animals infected with Mtb exhibit robust Ag-specific $CD4^+$ Th1 and $CD8^+$ T lymphocyte responses to Mtb Ags (1–3), implying that the initial steps in the priming and differentiation of T lymphocytes are functional in the setting of tuberculosis. However, since the early 20th century it has been known that Mtb is rarely, if ever, eliminated after infection (4–6).

A major challenge to developing more efficacious vaccines against tuberculosis is the incomplete understanding of the mechanism of immunity and the mechanism of immune evasion by Mtb. Despite strong evidence that in humans (7, 8) and mice (1) $CD4^+$ T lymphocytes with a Th1 phenotype (9, 10) are essential for preventing rapid progression of Mtb disease, little is known regarding the cellular mechanisms of the initiation of $CD4^+$ T cell responses following Mtb infection, and it is unclear how Mtb evades elimination once an adaptive immune response develops.

For >70 years (11) it has been known that Mtb survives within macrophages in the lungs, but it is unlikely that lung macrophages alone are capable of initiating cellular immune responses by activating Ag-specific naive $CD4^+$ T lymphocytes. Recently, dendritic cells (DCs) have been found to contain Mtb in human (12) and mouse (13) tissues, and the depletion of $CD11c^+$ cells (including DCs) in mice before an i.v. injection of Mtb delays the development of $CD4^+$ T cell responses and results in impaired immune control of Mtb (14). Although these data provide evidence that DCs can contain Mtb and that they can contribute to the timely development of protective immunity, the precise roles of DCs and macrophages in the trafficking of bacteria and initiation of immunity and as reservoirs of bacteria in tuberculosis remain undefined. Moreover, it is unclear how each of these cellular subsets interacts with Ag-specific T lymphocytes in lungs and lymph nodes to provide limited protective immunity in tuberculosis.

We developed a technique for sensitive and specific flow cytometry detection and phenotyping of cells from mice infected with GFP-expressing Mtb and found that DCs are infected with Mtb at high frequency in the lungs and draining lymph nodes after aerosol infection. We also found that DCs transport Mtb from the lungs to the local draining lymph node, but the frequency of transport decreases markedly after a peak in the 3rd week of infection. Moreover, we found that the subsets of cells that are infected at high frequency in vivo are poor stimulators of Mtb Ag-specific $CD4^+$ T cells despite expressing surface MHC class II and costimulatory molecules.

*Division of Infectious Diseases, Department of Medicine, New York University School of Medicine, New York, NY 10016; †Biomedical Sciences Graduate Program, University of California, San Francisco, CA 94143; ‡Department of Microbiology, Leprosy Research Center, National Institute of Infectious Disease, Tokyo, Japan; §Department of Microbiology and Immunology, Division of Immunology, Institute of Medical Science, University of Tokyo, Tokyo, Japan; ¶Department of Pathology and ‖Department of Microbiology, New York University School of Medicine, New York, NY 10016

Received for publication March 22, 2007. Accepted for publication June 5, 2007.

The costs of publication of this article were defrayed in part by the payment of page charges. This article must therefore be hereby marked *advertisement* in accordance with 18 U.S.C. Section 1734 solely to indicate this fact.

[1] This work was supported by National Institutes of Health Grant R01-AI051242 and by Special Coordination Funds for Promoting Science and Technology of the Ministry of Education, Culture, Sports, Science and Technology, Japan: Strategic Cooperation to Control Emerging and Reemerging Infections.

[2] Address correspondence and reprint requests to Dr. Joel D. Ernst, Division of Infectious Diseases, New York University School of Medicine, Smilow Research Center, Room 901, 550 First Avenue, New York, NY 10016; E-mail address: joel.ernst@med.nyu.edu or Dr. Kiyoshi Takatsu, Department of Microbiology and Immunology, Division of Immunology, Institute of Medical Science, University of Tokyo, 4-6-1 Shirokane-dai, Minato-ku, Tokyo, Japan; E-mail address: takatsuk@ims.u-tokyo.ac.jp

[3] Abbreviations used in this paper: Mtb, *Mycobacterium tuberculosis*; ADC, albumin dextrose catalase; β-gal, β-galactosidase; DC, dendritic cell; Tg, transgenic.

Materials and Methods

Mice

C57BL/6J mice were bred and housed in the New York University School of Medicine (New York, NY) animal facilities or purchased from The Jackson Laboratory. *plt/plt* (backcrossed against C57BL/6 for 10 generations, obtained from S. Luther and J. Cyster, University of California, San Francisco, CA), and P25 TCR-transgenic (Tg) mice were bred and housed in the New York University animal facility. Mice were infected at 8–12 wk of age.

Mtb strains and growth

Mtb (H37Rv) was transformed with the plasmid pMV262 encoding FACS-optimized GFPmut3 under the control of the *Mycobacterium bovis* BCG Hsp60 promoter (provided by Dr. L. Ramakrishnan, University of Washington, Seattle, WA). Bacteria were grown in Middlebrook 7H9 medium supplemented with 10% (v/v) albumin dextrose catalase (ADC) enrichment and 50 μg/ml kanamycin. Aerosol infection stocks were generated by initial passage in C57BL/6J mice. After 36 days of infection, lungs were homogenized and plated on Middlebrook 7H11 selective medium plates (Difco) with 50 μg/ml kanamycin and grown for 2–3 wk at 37°C. Bacterial colonies were scraped into Falcon T75 flasks containing 7H9$^+$ADC enrichment and grown lying flat to mid-log phase growth for ~7 days at 37°C. Bacteria were pelleted at 2000 $\times$ *g* and resuspended in one-tenth of the original growth volume of PBS containing 0.5% Tween 80, aliquoted, and frozen at −80°C. The aerosol stock titer was determined by preparing eight 10-fold serial dilutions of five random vials of stock in triplicate in PBS containing 0.5% Tween 80 and plating on Middlebrook 7H11 plates.

Antibodies

All Abs were purchased from BD Pharmingen unless otherwise stated. Anti-CD11c PerCP (H3L) was a custom conjugate from BD Pharmingen, and other Ab conjugates used were anti-CD11b allophycocyanin-Cy7, anti-Gr-1 allophycocyanin or PE-Cy7, and anti-CD86 allophycocyanin. Purified anti-CD80, anti-CD40, and anti-I-A/I-E were purchased from BD Pharmingen and conjugated to Alexa Fluor 647 by using a mAb conjugation kit from Molecular Probes.

Mouse aerosol infections

Mice were infected by the aerosol route using an inhalation exposure unit from Glas-Col. An aliquot of aerosol infection stock was thawed at room temperature, and the bacterial suspension was forced 10 times through a 25-gauge needle fitted to a 1-ml syringe to disperse clumps of bacteria. The inoculum was prepared by diluting the bacterial stock of a known concentration to a concentration equal to 2×10^4 times the intended dose per mouse in sterile water to yield 6 ml of inoculum. Five milliliters of the inoculum was loaded into the inhalation exposure unit nebulizer and the remaining 1 ml was used to confirm the inoculum concentration by serial dilution and plating on 7H11 agar. The following program was used to infect the mice: 900 s of preheating, 2400 s of nebulizing, 2400 s of cloud decay, and 900 s of decontamination. After infection, mice were returned to their original cages and housed in individually ventilated microisolator cages. For controls for the specificity of GFP fluorescence as a measure of infection, a group of C57BL/6J mice were infected with wild-type Mtb H37Rv by the same procedure within 24 h of the Mtb-GFP group. For all infections, the actual infection dose was determined by euthanizing five mice within 24 h of infection. Lungs were removed, homogenized, and plated on 7H11 agar plates. CFU were counted after incubation at 37°C for 2–3 wk.

Tissue harvests and CFU determination

Mice were euthanized by CO_2 followed by cervical dislocation. The lungs and mediastinal lymph nodes were removed and placed in digestion buffer (RPMI 1640, 5% FCS, and 10 mM HEPES). Tissues were minced using forceps and scissors into pieces 2-mm^3 in the greatest dimension. Tissue was then incubated in 1 mg/ml collagenase D (Roche) and 30 μg/ml DNase I (Roche) at 37°C for 45 min. Each tissue was forced through a 70-μm cell strainer (BD Falcon) and an aliquot was removed to determine the bacterial load. The single cell suspension was washed and the RBC were removed using ACK lysis buffer (155 mM NH_3Cl, 10 mM $KHCO_3$, and 88 μM EDTA). Live cells were counted using trypan blue exclusion.

FACS staining and acquisition

Staining for surface markers was done by resuspending 1×10^6 cells in medium with an Fc receptor-blocking Ab (clone 2.4G2) for 10 min at 4°C followed by washing and resuspension with FACS buffer (PBS, 1% FCS, 0.1% sodium azide, and 1 mM EDTA) containing Abs and incubation at 4°C for 20 min. Cells were then washed twice and fixed in 1% paraformaldehyde overnight at 4°C. Samples were acquired using a FACSDiva, LSR II, or FACSVantage flow cytometer depending on the experiment. Because Mtb-GFP$^+$ cells are rare, especially early in infection, and lung cells exhibit high autofluorescence, special conditions were required to detect and phenotype Mtb-GFP$^+$ cells. First, unstained lung cells from mice infected with wild-type Mtb H37Rv were used to set the boundary between the GFP$^+$ and negative populations. Second, due to the low frequency of GFP$^+$ cells, an abundant positive control was required to standardize the GFP compensation. For this purpose, RAW264.7 cells were transformed with the plasmid pEGFP-N1 (Clontech Laboratories) and a stable GFP-expressing line (RAW-GFP) was generated. RAW-GFP cells were spiked into a sample of unstained lung cells to compensate the GFP. Finally, because of the autofluorescence associated with lung cells it was not possible to use Abs conjugated to fluorophores spectrally adjacent to GFP. An empty/unused channel was necessary to establish a consistent GFP$^+$ gate. Mtb-GFP$^+$ cells could then be phenotyped using fluorophores with at least one spectral channel of distance from GFP.

Phenotyping and quantitation of lung and lymph node cells

CD11c^{high}CD11b^{high} lung cells were designated as myeloid DCs based on previously described functional and morphologic characteristics (15–17) and on the observation that, after aerosol infection of IFN-γR$^{-/-}$ mice with Mtb, they expressed high levels of surface MHC class II whereas in other lung cell subsets surface class II expression was markedly reduced in infected IFN-γR$^{-/-}$ mice (data not shown). Alveolar macrophages (CD11c^{high}CD11b^{low}) were identified by the pattern of staining of cells recovered by bronchoalveolar lavage and by the depletion of this cell subset from postlavage lung homogenates. Recruited macrophages (CD11c^{low}CD11b^{high}) were identified by their presence in low numbers in uninfected mice, their absence from bronchoalveolar lavage, the marked increase in their numbers in the lungs after aerosol infection with Mtb, and their dependence on IFN-γ responsiveness for the surface expression of MHC class II. Monocytes (CD11c$^-$CD11b^{low}) were also identified as in Ref. 15 and expressed low amounts of surface MHC class II in the presence or absence of IFN-γ responsiveness. Neutrophils were identified as described in *Results* on the basis of their nuclear morphology and the presence of myeloperoxidase. Myeloid DCs (CD11c^{high}CD11b^{high}) in mediastinal lymph nodes were identified as described (15, 16). CD11c$^+$CD11b^{low} lymph node cells, despite their resemblance in terms of expression of these markers, were considered to be distinct from alveolar macrophages in the lung because they are present in lymph nodes that do not drain the lungs. They and the CD11c$^+$CD11b$^-$ cells are likely to be similar, if not identical, to DC subsets previously identified in mouse lymph nodes (18, 19).

Mtb expressing β-galactosidase (β-gal) and immunohistochemistry

Mtb H37Rv was transformed with the plasmid pUS989 (a gift from Dr. D. McIntosh, Oswaldo Cruz Foundation, Rio de Janeiro, Brazil), which expresses β-galactosidase under the control of the Hsp60 promoter (20), to prepare a strain termed Mtb-β-gal. Wild-type C57BL/6 mice were infected with mouse-passaged Mtb-β-gal by the aerosol route as described above. At designated time points lungs were inflated with Tissue-Tek OCT (Sakura Finetek) and embedded and frozen in Tissue-Tek OCT. Samples were stored at −80ºC. Tissue was sectioned into 6-μm sections using a Leica cryostat fitted with a CryoJane tape-transfer system and a Cryo-Vac-Away system (Instrumedics). Sections were dried and fixed for 10 min with acetone. Mtb-β-gal was detected in sections by staining with a solution of 1 mM $MgCl_2$, 5 mM potassium ferrocyanide, 5 mM potassium ferricyanide, and 1 mg/ml X-galactosidase in PBS for 12 h at 37°C. Immunohistochemistry was performed using a mAb to DEC-205 (NLDC-145; Serotec), which was detected using biotin-labeled anti-rat IgG (Vector Laboratories) and a Vector ABC alkaline phosphatase kit using Vector Red as the substrate (Vector Laboratories). Sections were counterstained with Vector hematoxylin and mounted using Permount. Sections were viewed and photographed using a Leica DMRB microscope using a ×20 or a ×100 oil objective and equipped with a Diagnostics Instruments Spot Slider camera and Spot software.

Cell sorting and microscopy

Paraformaldehyde-fixed, single-cell suspensions of lung and lymph nodes were stained with 4′,6′-diamidino-2-phenylindole (Molecular Probes) and ~1000 cells were sorted onto slides based on CD11b and CD11c surface stains using a FACS Vantage (New York University Center for AIDS Research, New York NY). Cells were mounted using Slow-Fade mounting

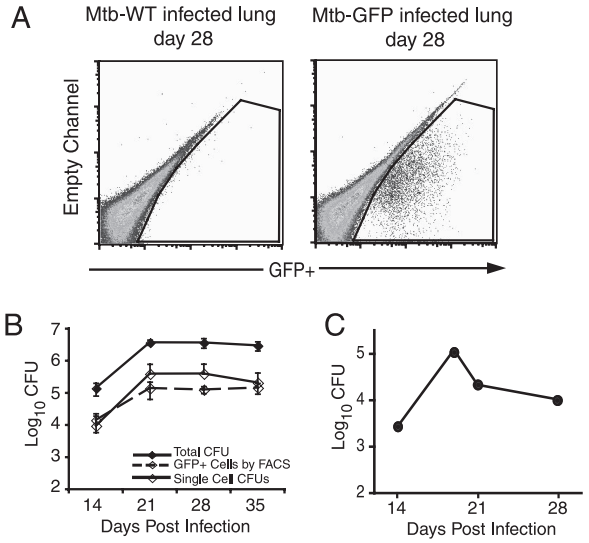

FIGURE 1. Flow cytometry detection of Mtb-GFP-infected cells from mouse lung tissues. *A*, Flow cytometry dot plots showing single-cell suspensions from the lungs of mice infected with wild-type Mtb H37Rv (Mtb-WT; *left panel*) or GFP-expressing Mtb H37Rv (*right panel*) 28 days postinfection, confirming that GFP^+ cells are only found in mice infected with Mtb-GFP. *B*, Quantitation of infection by comparison of the number of infected cells as determined by flow cytometry (—◆—) and bacterial CFU in total lung homogenate (—◇—) and in washed lung cells (- - -◇- - -). GFP^+ was calculated as the percentage of GFP^+ cells determined by flow cytometry multiplied by the total number of cells in the single-cell suspension. For total homogenate CFU, an aliquot of total disrupted lung tissue before any washing was serial diluted and plated on 7H11 agar in triplicate. For single-cell suspension CFU, an aliquot of the final single-cell preparation from the lung used to determine the total cell number was serial diluted without lysing the cells and plated on 7H11 agar in triplicate. Colonies were counted 14–21 days later. Data are the mean ± SD of five mice per time point. *C*, Bacterial load in the mediastinal lymph node was assessed by serial dilution of the total homogenate before any washing and plating on 7H11 agar from the experiment displayed in Fig. 3.

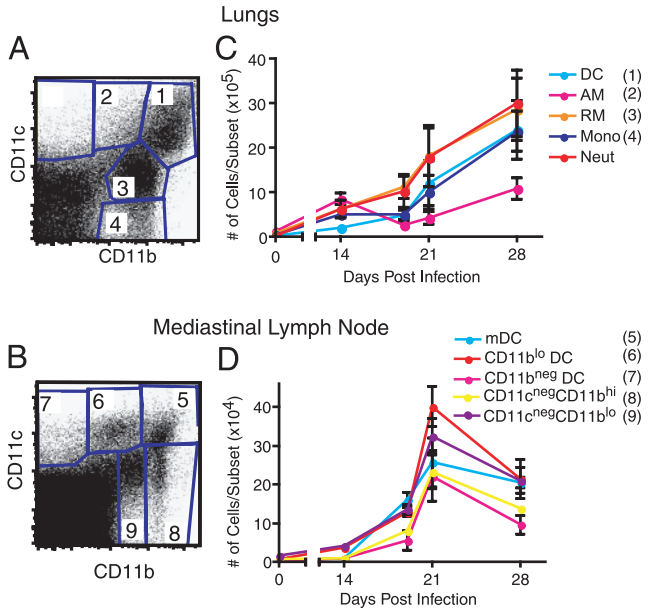

FIGURE 2. *A* and *B*, Flow cytometry dot plots of the distribution of CD11c- and CD11b-expressing cell subsets in the lungs (*A*) and the mediastinal lymph node (*B*) before (day 0) and after aerosol infection. *C* and *D*, The total number of cells in each of the CD11c/CD11b-defined subsets before (day 0) and during the course of infection in the lungs (*C*) and mediastinal lymph node (*D*). mDC, Myeloid DC; RM, recruited interstitial macrophage; AM, alveolar macrophage; Mono, monocyte; Neut, neutrophil. The neutrophil subset is not shown on the dot plot because it was excluded by gating on $CD11c^-Gr\text{-}1^{high}$ cells before identifying the CD11c/CD11b-defined subsets. Cell numbers were calculated by multiplying the percentage of cells in each subset obtained through flow cytometry by the total number of cells determined through manual count of the total number of cells in the single cell suspension from each tissue. Data are shown as mean ± SD for three (lymph nodes) or five (lungs) mice per time point. Cell populations in lungs of uninfected mice were ($\times 10^4$): myeloid DC, 2.2 ± 0.5; alveolar macrophage, 13 ± 3; recruited interstitial macrophage, 9.1 ± 2.1; monocytes, 5.3 ± 1.6; neutrophils, 1.9 ± 0.9. Cell populations in mediastinal lymph nodes of uninfected mice were ($\times 10^3$): myeloid DC, 4.1 ± 0.2; $CD11b^{low}$DC, 7.4 ± 0.1; $CD11b^-$DC, 2.5 ± 0.1; $CD11c^-CD11b^{high}$, 8.0 ± 0.2; $CD11c^-CD11b^{low}$, 18 ± 0.3.

medium (Molecular Probes) and visualized with a ×100 oil immersion objective on a Leica DMRB fluorescent microscope. Photomicrographs were recorded using a Spot Slider digital camera and Spot Software.

Stimulation of Mtb-specific $CD4^+$ T lymphocytes by cells from Mtb infected mice

T cells and B cells were removed from single cell suspensions of lungs and lymph node using Dynal magnetic bead selection (Invitrogen) to enrich for APCs. For live sorts, cells were stained in sterile PBS with 10% FCS, kept on ice, and sorted using a FACS Vantage at the New York University Center for AIDS Research. $CD4^+$ T cells were isolated from P25 TCR-Tg mice (21) by using a CD4 T cell isolation kit and an autoMACS system (Miltenyi Biotec). $CD4^+$ T cells ($1–2 \times 10^5$) were combined with sorted APCs at designated ratios in complete medium (RPMI 1640, 10% FCS, L-glutamine, nonessential amino acids, sodium pyruvate, HEPES, and 2-ME) in the presence of 10 μg/ml P25 TCR-specific peptide (Mtb Ag 85B aa 240–254, FQDAYNAAGGHNAVF; synthesized by Invitrogen Life Technologies) for 3 days at 37°C with 5% CO_2. Supernatants were assayed in triplicate for IFN-γ by ELISA (BD Biosciences).

CIITA-RAW264.7 cell Ag presentation assay

The FLAG epitope and open reading frame of human CIITA III were excised from p3FgCIITA8 (provided by Dr. J. Ting, University of North Carolina, Chapel Hill, NC) by using *Eco*RI and ligated into pQCXIN (Clontech Laboratories). The product was used to transfect GP2-293 cells, together with pVSV-G, to prepare vesicular stomatitis virus G protein-pseudotyped retroviral particles for the constitutive expression of CIITA and neo^r as a bicistronic message driven by the CMV immediate-early promoter with a viral internal ribosome entry site for the translation of neo^r. Packaged retroviral particles were used to transduce RAW264.7 cells, stably transduced cells were selected in G418, and individual clones were characterized by their levels of expression of surface MHC class II by FACS. A clone that expressed surface class II at a level that resembled that of mature bone marrow-derived DCs was expanded and used for subsequent studies.

For Ag presentation experiments, CIITA-RAW cells were grown in RPMI 1640 medium with 10% heat-inactivated FCS and 2 mM L-glutamine and plated at a density of 2.5×10^6 cells per 10-cm tissue culture dish. Mtb (H37Rv) was grown in Middlebrook 7H9 broth supplemented with ADC enrichment to an OD_{580} of 0.5–1.0. The culture was centrifuged at 2,200 × *g* for 10 min and the pellet was resuspended in 2 ml of RAW cell growth medium. Clumps of bacteria were disrupted by vortexing on high for 3 min in the presence of 3-mm glass beads and passed through a 5-μm syringe filter (Millipore) by gravity flow to remove clumps. Bacterial density was determined by counting in a Petroff-Hausser counter and confirmed by serial dilution and plating on 7H11 agar. CIITA-RAW cells were infected at a multiplicity of infection of 10 or treated with 200 ng/ml gamma-irradiated H37Rv for 18–24 h. CIITA-RAW cells were scraped and harvested in PBS with 5 mM EDTA and replated in a round-bottom 96-well plate at designated densities in triplicate in complete medium (RPMI 1640 medium, 10% heat-inactivated FCS, 10 mM HEPES, 100 μM nonessential amino acids, 1 mM sodium pyruvate, 100 U/ml penicillin, 100 μg/ml streptomycin sulfate, and 1× 2-ME). Cells were incubated with 1 μM OVA peptide (aa 323–339) (Peptides International) for 6 h and then fixed for 10 min with 1% paraformaldehyde and thoroughly washed with PBS. DO11.10 $CD4^+$ T cells that had been primed for 4 days in the presence of 1 ng/ml IL-12, 1 μM OVA peptide (323–339), and 10 μg/ml

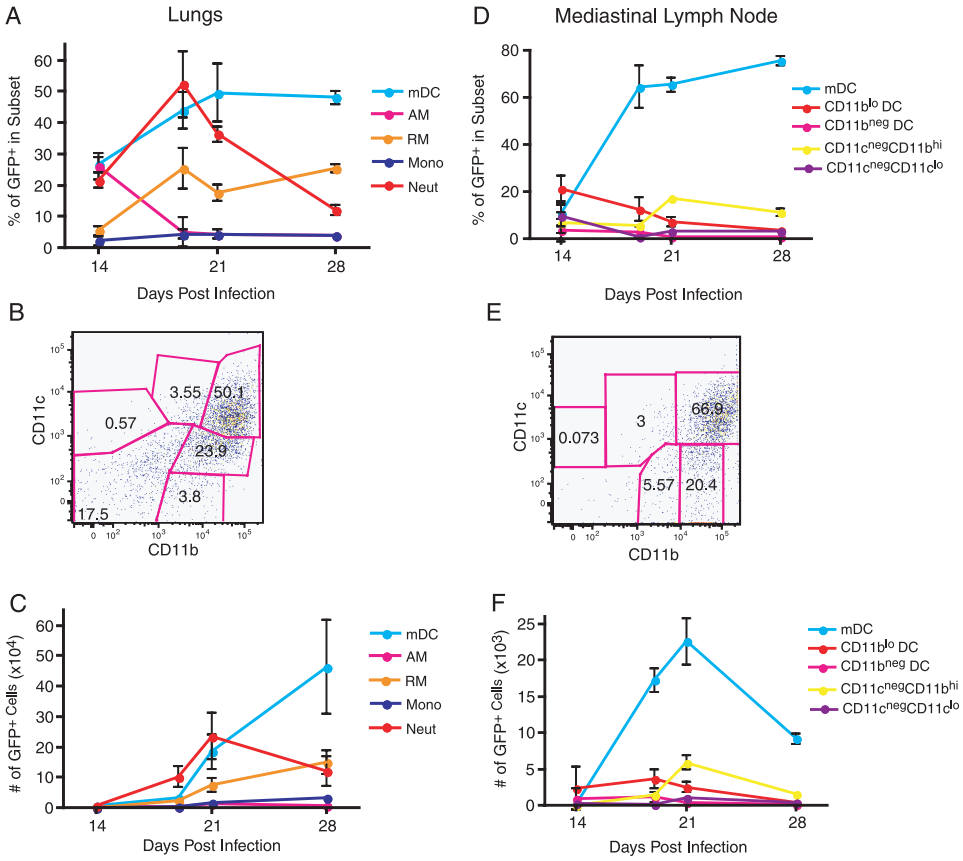

FIGURE 3. Distribution of Mtb-GFP infected cells in the CD11c/CD11b-defined leukocyte subsets of the lung and mediastinal lymph node. *A* and *D*, Percentage of GFP^+ cells that fall within each of the subsets of leukocytes in the lung (*A*) and mediastinal lymph node (*D*) during the course of infection. *B* and *E*, Flow cytometry dot plot of the distribution of GFP^+ cells in the lung (*B*) and mediastinal lymph node (*E*) at day 28 postinfection on a plot of CD11c vs CD11b. The gates represent the subsets of APCs identified in each tissue based on the surface expression of CD11c and CD11b. Fewer than 5% of the $CD11c^+$ cells in the lungs expressed either CD3 or CD8α, and Mtb-GFP were not detected in any $CD11c^+CD3^+$ or $CD11c^+CD8\alpha^+$ cells (not shown). The numbers in the gates represent the percentage of GFP^+ displayed in that gate. *C* and *F*, The total number of infected cells within the leukocyte subsets in the lung (*C*) and mediastinal lymph node (*F*) during the first 4 wk of infection. The total number of infected cells in each subset was determined by multiplying the percentage of the total cells that are GFP^+ within each subset as determined through flow cytometry by the total number of cells isolated from the tissue at each time point. Data shown are mean ± SD for five mice per time point. mDC, Myeloid DC; RM, recruited interstitial macrophage; AM, alveolar macrophage; Mono, monocyte; Neut, neutrophil.

anti-IL-4 were purified using a $CD4^+$ isolation kit and an autoMACS machine, added to the CIITA-RAW cells at 2×10^5 in complete medium, and incubated at 37°C and 5% CO_2 for two days. Supernatants were harvested and assayed in triplicate using ELISA with anti-mouse IFN-γ Abs (BD Biosciences), and absorbance was read on a microplate reader (Bio-Tek Instruments).

Statistical analysis

Statistical comparison of the number of bacteria per cell in myeloid DCs and recruited macrophages was performed by the Mann-Whitney *U* test and a comparison of the number of DCs and bacteria in lymph nodes of wild-type and *plt/plt* mice was performed by unpaired Students' *t* test, both using both Prism 4 for Macintosh (version 4.0a) from GraphPad Software.

Results

Flow cytometry detection of Mtb-infected cells from mouse tissues

To identify, characterize, and quantitate Mtb-infected cells in a temporal fashion during infection, we performed flow cytometry analysis on the lungs of mice infected with Mtb constitutively expressing GFP (Mtb-GFP). We first confirmed the specificity of detection by determining that green fluorescent events were detected in cells from mice infected with Mtb-GFP but not in cells from mice infected with wild-type Mtb (Fig. 1*A*). To confirm that

Table I. *Percentage of cells in each cell subset from the lungs that are GFP^+ over the course of infection*[a]

	Dendritic Cells	Alveolar Macrophages	Recruited Macrophages	Monocytes	Neutrophils
14	1.89 ± 0.99	0.77 ± 0.21	0.63 ± 0.28	0.11 ± 0.07	1.26 ± 0.77
19	10.14 ± 0.84	2.07 ± 0.36	4.88 ± 1.32	1.21 ± 0.41	9.09 ± 2.09
21	16.2 ± 1.82	4.09 ± 0.97	7.86 ± 2.71	2.76 ± 1.32	12.86 ± 3.62
28	15.63 ± 2.95	2.79 ± 0.4	6.82 ± 2.13	1.91 ± 0.43	3.52 ± 0.57

[a] Results shown are mean ± SD from analysis of five mice.

Table II. *Percentage of cells in each cell subset from the mediastinal lymph node that are GFP$^+$ over the course of infection*[a]

	Myeloid DC	CD11c$^+$CD11b^{low}	CD11c$^+$CD11b$^-$	CD11c$^-$CD11b^{high}	CD11c$^-$CD11b^{low}
14	2.83	1.51	1.69	1.17	0.13
19	8.22	0.40	0.15	0.87	0.0095
21	6.78	3.25	4.97	1.73	0.07
28	3.44	0.21	0.029	1.15	0.03

[a] Numbers were obtained by pooling cells from lymph nodes from five mice at each time point.

these green fluorescent events represented Mtb-GFP infected cells, we sorted cells in the positive and negative gates in the infected lung (Fig. 1*A*, *right panel*) and found that >90% of the cells in the positive gate contained one or more bacteria whereas <0.002% of the cells in the negative gate contained bacteria as detected by fluorescence microscopy.

We next monitored the numbers of Mtb-GFP$^+$ cells over several weeks of infection. First, we confirmed that the infection was progressing as expected by plating whole homogenates of total lung tissue for viable bacteria (Fig. 1*B*). We found the expected increase in bacterial counts from 14 to 21 days followed by a plateau in the number of bacteria. The number of fluorescent events per lung detected by flow cytometry displayed the same temporal pattern as the total bacterial counts (Fig. 1*B*). We consistently detected ~1 $\log_{10}$ fewer fluorescent events than viable bacteria (Fig. 1*B*). This difference is partially due to the loss of bacteria during the washing steps that were performed before FACS analysis as determined by assessing the CFU in the supernatant of each wash (data not shown). In addition, microscopic examination of sorted cells showed that many infected cells contained more than one bacterium (see below), resulting in a ratio of GFP$^+$ events to CFU of <1. Additionally, the number of fluorescent events detected correlated very closely with the number of viable bacteria detected in the washed, single-cell suspensions that were not lysed with detergent before plating (Fig. 1*B*). Taken together, these data indicate that our flow cytometry technique is both sensitive and specific for detecting infected cells and show that the number of infected cells first increases and then plateaus, mirroring the pattern of total bacterial counts. This indicates that during the initial phase of infection with Mtb before the appearance of the adaptive immune response, the growth of the bacterial population in the lungs is accompanied by an expansion of the number of infected cells, which implies a high rate of cell-to-cell spread of the bacteria. This cell-to-cell spread is diminished by the adaptive immune response, as the number of infected cells plateaus with the same kinetics as the bacterial population size.

Mtb infects lung cells with diverse phenotypes in vivo

Differential quantitative expression of the leukocyte markers CD11b and CD11c, together with bronchial lavage, identified three major and two minor subsets of myeloid cells in the lungs (15–17) (Fig. 2). At the earliest time point that Mtb-GFP could be reliably detected (14 days postinfection), alveolar macrophages, myeloid DCs, and neutrophils were the predominant infected cells in the lungs (Fig. 3). By 19 days postinfection myeloid DCs and interstitial macrophages were recruited to the lungs and outnumbered the alveolar macrophages (Fig. 2). Concurrent with their recruitment to the lungs, myeloid DCs and recruited interstitial macrophages became infected (Fig. 3) and were the predominant populations of infected cells in the lungs while alveolar macrophages, which changed minimally in total number during the course of infection, decreased as a fraction of the total infected cells in the lungs. We confirmed that GFP$^+$ cells in each of these cell subsets represented Mtb-infected cells by flow sorting of each subset, followed by examination of the sorted cells by fluorescence microscopy. Myeloid DCs and recruited macrophages remained the predominant infected cells in the lungs throughout the remainder of the monitored infection. Despite the long-standing belief that macrophages represent the resident cells for Mtb, myeloid DCs account for the largest percentage (>50%) of infected cells in the lung after 14 days of infection. Although recruited interstitial macrophages represent a significant percentage of the infected cells, infected myeloid DCs outnumber infected recruited macrophages by 2:1 at the peak of the infection in the lung (Fig. 3, *A* and *C*). Although accounting for approximately half the infected cells after 3 wk, the myeloid DCs only represent 6.8% of the total cells in the lung; therefore, a high proportion of the DCs in the lung become infected with Mtb (Tables I and II).

In addition to macrophages and DCs, between 14 and 21 days postinfection we found GFP$^+$ cells within a CD11c$^-$CD11b^{high}Gr-1^{high} population. Examination by microscopy of flow-sorted GFP$^+$ cells from this population confirmed that the GFP$^+$ cells contained Mtb, histological staining by Hema3 showed that 80% of the cells possessed granulocyte-like nuclei, and 72% of the cells were strongly positive for myeloperoxidase activity by Leder stain. Taken together, these results indicate that granulocytes are transiently infected with Mtb early in infection but that they represent a minor fraction of the infected cells at later times.

DCs transport Mtb to the mediastinal lymph node

We also used flow cytometry to characterize the cells in the mediastinal lymph node, which drains the lungs. After day 14 postinfection, one population of cells dominated the distribution of infected cells in the mediastinal lymph node (Fig. 3, *D–F*). Greater than 65% of the infected cells were CD11c^{high}CD11b^{high} myeloid DCs, which resemble the predominant infected cell population in the lungs. The total number of these cells increased progressively in the lymph node during the course of infection (from 1×10^4 to

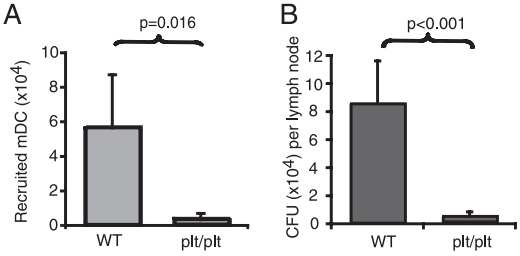

FIGURE 4. DCs and Mtb CFU in lymph nodes of C57BL/6J and *plt/plt* mice 14 days after aerosol infection with ~100 Mtb CFU/mouse. *A*, Recruitment of myeloid DCs, calculated as the increase in myeloid DCs in the mediastinal lymph node in response to Mtb infection of wild-type and *plt/plt* mice relative to the number of myeloid DCs in uninfected lymph nodes from each strain of mice. *B*, Mtb CFU in the mediastinal lymph node. Data represents the mean ± SD of at least five mice in each group. WT: Wild-type C57BL/6 mice.

Table III. *APC subsets in mediastinal lymph nodes of wild-type and plt/plt mice before and 14 days after M. tuberculosis infection*[a]

	C57BL/6				*plt/plt*			
	Uninfected		Day 14		Uninfected		Day 14	
Cell Subset	Percentage (%)	$\times 10^4$	Percentage (%)	$\times 10^4$	Percentage (%)	$\times 10^4$	Percentage (%)	$\times 10^4$
Total Cells		182		950		50		54.8
Total APC	7.91	14.4 ± 0.4	4.7	44.8 ± 22.5	5.43	2.72	7.76	4.2 ± 2.1
Myeloid DC	0.83	1.5 ± 0.1	0.54	4.9 ± 3.8	0.57	0.29	0.95	0.5 ± 0.4
$CD11b^{low}$ DC	1.48	2.7 ± 0.02	0.96	9.4 ± 5.6	0.61	0.31	1.36	0.7 ± 0.4
$CD11b^{-}$ DC	0.49	0.9 ± 0.05	1.04	9.9 ± 6.7	0.55	0.28	2.32	1.2 ± 1.0
$CD11c^{-}CD11b^{high}$	1.59	2.9 ± 0.1	0.56	5.1 ± 2.9	1.56	0.78	0.75	0.42 ± 0.3
$CD11c^{-}CD11b^{low}$	3.52	6.4 ± 0.2	1.6	15.4 ± 8.5	2.15	1.08	2.38	1.3 ± 0.7

[a] Data from uninfected *plt* mice were obtained by pooling cells from lymph nodes of five mice; the remaining data are mean ± SD of five mice per group.

2×10^5), and by day 19 ~25% of these cells in the mediastinal lymph node contained bacteria detectable by flow cytometry. In contrast to the total number of myeloid DCs in the mediastinal lymph node, the number of infected myeloid DCs reached a peak of $\sim 2.5 \times 10^4$ by day 21 postinfection and then decreased to $\sim 8 \times 10^3$ per lymph node by day 28. The number of viable bacteria in the lymph node decreased by a similar extent between days 21 and 28.

Infected lymph node cells could arise by several different mechanisms, including the drainage of cell-free bacteria from the lungs in lymphatic fluid, the phagocytosis of hematogenously spread bacteria by resident cells in the lymph node, or the transport by DCs that become infected in the lungs and then migrate to the lymph node when they mature. To distinguish these possibilities we infected *plt* mice that lack the expression of CCL19 and CCL21ser (22), which are normally expressed in the lymphatic endothelium and the paracortical zone of lymph nodes and serve as ligands for CCR7 on mature DCs. Compared with wild-type controls, mediastinal lymph nodes of *plt* mice recruited 95% fewer $CD11c^{high}CD11b^{high}$ cells and contained 95% fewer bacteria on day 14 after Mtb infection (Fig. 4). The number of lung DCs or macrophages and the number of bacteria in the lungs did not differ significantly on day 14 between *plt* mice and controls. Although the recruitment of other APC subsets to the mediastinal lymph node was also defective in Mtb-infected *plt* mice (Table III), the defective migration of myeloid DCs is most likely to account for the lower number of bacteria in the lymph node because this subset represents the largest fraction of infected cells in the lymph node. These results support the hypothesis that mature DCs transport live Mtb from the lungs to the local draining lymph node, at least during the early phase of infection. The observation that the number of Mtb-infected myeloid DCs in the lymph node decreases later in infection while the number of infected myeloid DCs in the lungs remains at the high level achieved by day 21 (Fig. 3) implies that migration of Mtb-infected myeloid DCs from the lungs to the mediastinal lymph node is a transient phenomenon and is down-regulated in the later stages of infection.

Immunohistochemistry localizes Mtb in DEC-205$^+$ cells

As an alternative approach to determining the frequency of Mtb infection of DCs, we used immunohistochemistry and a well-characterized Ab to the DC marker DEC-205. Because immunohistochemistry staining and acid-fast staining of mycobacteria are incompatible, we performed these studies using a strain of Mtb transformed with a plasmid for constitutive expression of *Escherichia coli* β-gal. This revealed that bacteria could be detected in DEC-205$^+$ as well as DEC-205$^-$ cells in pulmonary granulomas and that infected DEC-205$^+$ cells formed aggregates with other infected DEC-205$^+$ cells while infected DEC-205$^-$ cells clustered with other DEC-205$^-$ cells (Fig. 5). When we quantitated the frequency of Mtb in DEC-205$^+$ cells in the lungs we found that 21 days after infection 53% of the bacteria were in DEC-205$^+$ cells; this increased to 63% by 28 days after infection. These results support the observations obtained by flow cytometry that the majority of bacteria reside in lung cells with the characteristics of DCs.

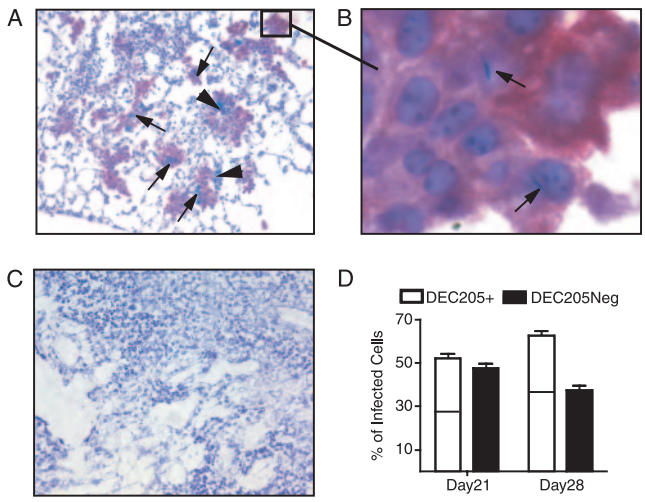

FIGURE 5. Immunohistochemical localization of Mtb in DEC-205$^+$ and DEC-205$^-$ lung cells. Mtb-β-gal was visualized with X-galactosidase (blue-green) and DEC-205 (red) was visualized with the mAb NLDC-145 in hematoxylin-counterstained (blue) lung sections from a mouse infected by the aerosol route 28 days earlier. *A*, Original magnification: ×20; arrows designate bacteria in DEC-205$^+$ cells and arrowheads designate bacteria in DEC-205$^-$ cells. *B*, Original magnification: ×100 with oil immersion. *C*, Isotype control stained lung, counterstained with hematoxylin. *D*, On days 21 and 28 postinfection Mtb-β-gal was scored for its localization in DEC-205$^+$ or DEC-205$^-$ cells in lung sections. DEC-205$^+$ cells were further categorized as staining with high (*lower section* of bar) or low (*upper section* of bar) intensity. At each time point the distribution of Mtb-β-gal was determined in cells on six lung sections; the percentage of bacteria in DEC205$^+$ and DEC-205$^-$ cells was calculated for each section; data shown are mean ± SD for the six sections from each time point. On sections from day 21, a total of 525 Mtb-β-gal$^+$ cells were counted; on sections from day 28, a total of 722 Mtb-β-gal$^+$ cells were counted.

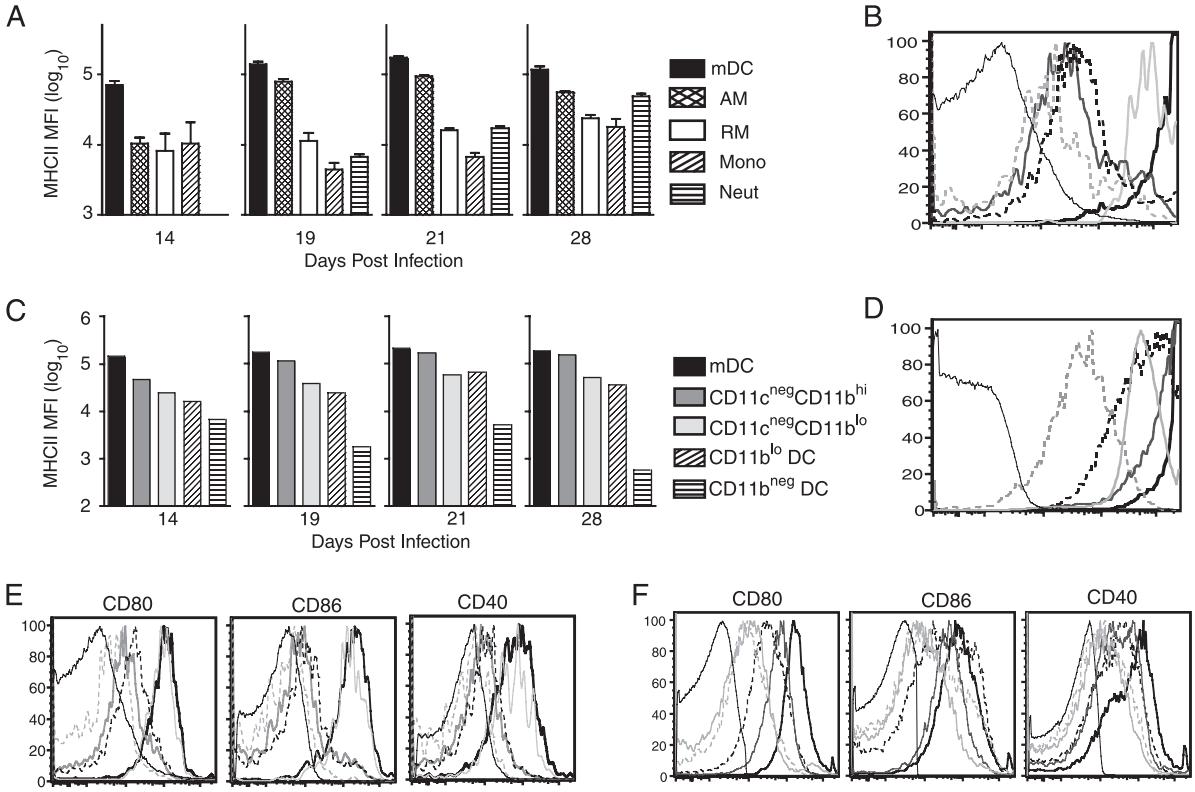

FIGURE 6. Expression of surface MHC class II on Mtb-GFP-infected cells in the CD11c/CD11b-defined subsets of leukocytes in the lung and mediastinal lymph node. *A*, MHC class II mean fluorescence intensity of the GFP$^+$ cells within each cell subset during the first 4 wk of infection. Data shown are mean ± SD for five mice per time point. mDC, Myeloid DC; RM, recruited interstitial macrophage; AM, alveolar macrophage; Mono, monocyte; Neut, neutrophil. *B*, Histogram of MHC class II expression on lung cell subsets from a representative mouse 21 days postinfection. Bold black line, Myeloid DC; dark gray line, alveolar macrophage; light gray line, recruited interstitial macrophage; dashed gray line, monocyte; heavy dashed line, neutrophil; fine black line, control. *C*, MHC class II MFI for the GFP$^+$ cells within each of the CD11c/CD11b-defined cell subsets in the mediastinal lymph node. Cells from the mediastinal lymph nodes of five mice per time point were pooled into a single sample to acquire sufficient GFP$^+$ events for quantitation. *D*, Histogram of MHC class II expression on lymph node cell subsets from a representative mouse 21 days postinfection. Bold black line, Myeloid DC; heavy dashed line, CD11b^{low} DC; dashed gray line, CD11b$^-$ DC; dark gray line, CD11c$^-$CD11b^{high}; light gray line, CD11c$^-$CD11b^{low}; fine black line, control. *E* and *F*, Representative histograms of costimulatory molecule expression on each APC subset from the lung (*E*) and mediastinal lymph node (*F*) 21 days postinfection. Cell subsets are designated as in *B* and *D*. Expression of MHC class II on all CD11c/CD11b-defined subsets in the lungs and lymph nodes of uninfected mice was below the lower limit of the scale shown in *A* and *C*.

APCs in the lungs and mediastinal lymph nodes of Mtb-infected mice express surface MHC class II and costimulatory molecules

Secondary lymphoid tissues such as lymph nodes are the sites of the priming of naive CD4$^+$ T lymphocytes by MHC class II-restricted recognition of peptide Ag, usually on DCs. In the lungs, Ag presentation is necessary for recognition of infected cells by Mtb Ag-specific effector CD4$^+$ T cells. Our finding that Mtb infects DCs in the lungs and mediastinal lymph node indicates that these cells contain Mtb Ag and may participate in the activation of naive (lymph node) and effector (lung) CD4$^+$ T cells. We found that myeloid DCs from the lungs and the mediastinal lymph nodes of Mtb-infected mice expressed high levels of MHC class II (Fig. 6). DCs in the lungs of infected mice expressed progressively higher levels of surface MHC class II from 14 to 21 days after infection, consistent with progressive maturation of resident and newly recruited DCs by bacterial products and by proinflammatory cytokines induced by infection (23, 24). Likewise, myeloid DCs in the mediastinal lymph node expressed high levels of MHC class II, consistent with maturation. Further evidence for the maturation of DCs in the lungs and mediastinal lymph node was provided by the expression of costimulatory molecules (CD80, CD86, and CD40) on a higher proportion of lung and mediastinal lymph node DCs

Table IV. *Percentage of GFP$^+$ cells in each lung cell subset that express costimulatory molecules*[a]

	CD86			CD80		CD40	
Subset	Day 14	Day 21	Day 28	Day 14	Day 28	Day 14	Day 28
Myeloid DC	73.8 ± 7.32	91.6 ± 1.38	53.9 ± 1.82	97.4 ± 2.78	83.3 ± 1.78	40.8 ± 9.65	72.1 ± 3.07
Alveolar Macrophage	35.5 ± 8.94	92.8 ± 0.96	74 ± 6.48	94.1 ± 3.91	86.3 ± 2.03	6.68 ± 2.56	73.5 ± 8.29
Recruited Macrophage	51.7 ± 18.3	27 ± 3.7	28.9 ± 3.36	71 ± 14.1	47.8 ± 5.51	36.1 ± 13.7	21.1 ± 3.88
Monocyte	17.9 ± 12.5	13.9 ± 2.31	8.29 ± 2.33	38.8 ± 38.8	16.5 ± 7.24	17.35 ± 4.85	3.19 ± 0.4
Neutrophil	78.3 ± 6.95	27.4 ± 2.56	9.87 ± 1.94	89.5 ± 7.74	21.8 ± 3.29	75.6 ± 3.63	15.2 ± 3.04

[a] Results shown are mean ± SD from analysis of five mice at each time point.

Table V. *Percentage of total (GFP$^+$ and GFP$^-$) lung cells in each subset that express costimulatory molecules*[a]

Subset	CD86			CD80		CD40	
	Day 14	Day 21	Day 28	Day 14	Day 28	Day 14	Day 28
Myeloid DC	62.3 ± 5.64	85.1 ± 3.48	65.4 ± 1.64	54.4 ± 20.9	83.1 ± 1.08	32.4 ± 10.1	57.2 ± 1.38
Alveolar Macrophage	36.9 ± 4.24	88.9 ± 1.52	71.1 ± 2.64	80.7 ± 10.4	87.5 ± 0.64	3.33 ± 2.23	27.2 ± 3.17
Recruited Macrophage	41.2 ± 5.82	45 ± 4.66	28.1 ± 4.48	62.4 ± 9.3	46.8 ± 3.5	33.9 ± 2.79	11.9 ± 0.39
Monocyte	19.4 ± 5.94	31 ± 2.06	13.8 ± 2.27	27.7 ± 10.5	23.3 ± 3.61	7.24 ± 2.52	3.5 ± 0.44
Neutrophil	76.1 ± 5.99	33.7 ± 4.26	6.67 ± 0.91	87.7 ± 5.06	11.7 ± 1.41	73.1 ± 3.63	3.18 ± 0.34

[a] Results shown are mean ± SD from analysis of five mice at each time point.

(Tables IV and V). Consistent with other studies in mice (15) and humans (25), we found that alveolar macrophages also expressed high levels of MHC class II, although the levels were not as high as those on DCs. By comparison, newly recruited interstitial macrophages, which represent a major subset of the Mtb-infected cells in the lungs, expressed lower levels of MHC class II as reflected by 10-fold lower fluorescence intensity by flow cytometry, and a lower proportion of these cells expressed CD80 and CD86 (Fig. 6 and Tables IV and V).

Subsets of cells from tissues of Mtb-infected mice differ in their ability to stimulate Mtb-specific CD4$^+$ T lymphocytes

The differences in expression of MHC II and costimulatory molecules on distinct subsets of cells from Mtb-infected mice suggested that cells in the subsets might differ in their capacity to stimulate CD4$^+$ T lymphocytes. To test this hypothesis, we sorted lung and mediastinal lymph node cells on the basis of their quantitative expression of CD11b and CD11c and used the sorted cells to stimulate T cell Ag receptor (TCR) Tg (P25 TCR-Tg) CD4$^+$ T cells that recognize a peptide from Mtb Ag 85B (21).

In the lymph node, we expected that the myeloid DCs from Mtb-infected mice would be the most efficient APCs to CD4$^+$ T cells because they exhibit a mature phenotype and are well known for their efficiency as APCs. However, we found that myeloid DCs from mediastinal lymph nodes of Mtb-infected mice were poorer APCs than were CD11c^{high}CD11b$^{low/-}$ DCs, which elicited twice as much IFN-γ from the responding T cells as than did myeloid DCs (Fig. 7*A*). The same pattern was observed for the stimulation of IL-2 secretion, indicating that the differential ability of the APC subsets was not confined to a single T cell response (not shown). When we compared the ability of the same subsets of DCs (after maturation with TNF and LPS) from lymph nodes of uninfected mice to stimulate P25 TCR-Tg cells, myeloid DCs were the most efficacious in stimulating the production of IFN-γ from the responding T cells (data not shown). Because myeloid DCs are the predominant Mtb-infected cells in the lymph node and nonmyeloid DCs are infected with very low frequency, these results suggest that Mtb infection may inhibit direct Ag presentation by myeloid DCs.

Among the cells in the lungs, we also anticipated that myeloid DCs would be efficient APCs because they express the highest levels of surface MHC class II and costimulatory molecules. However, as in the mediastinal lymph nodes, myeloid DCs isolated from the lungs stimulated P25 TCR-Tg CD4$^+$ cells poorly. Indeed, myeloid DCs isolated from the lungs of Mtb-infected mice stimulated the CD4$^+$ T cells no more effectively than did recruited macrophages, which express lower levels of MHC II and costimulatory molecules (Fig. 7*B*). In contrast, alveolar macrophages, which represent a small percentage of the total of the infected cells, consistently elicited the greatest amount of IFN-γ from P25 TCR-Tg CD4$^+$ T cells. In comparison to mediastinal lymph node cells with comparable surface phenotypes, all of the subsets of cells from the lungs were less efficacious stimulators of CD4$^+$ T cells.

Mtb inhibits MHC class II Ag presentation without reducing surface class II expression

The finding that cells from Mtb-infected mice were poor stimulators of Ag-specific CD4$^+$ T cells suggested that Mtb infection might inhibit class II Ag presentation. To test this hypothesis, we constructed a cell line that constitutively expresses high levels of surface MHC class II and other mediators of class II Ag presentation due to the constitutive expression of CIITA. These cells were efficient APCs to DO11.10 OVA-specific TCR-Tg CD4$^+$ T lymphocytes (Fig. 8). When these cells were infected with live, virulent Mtb, their stimulation of DO11.10 cells was reduced by 90% without a significant change in their surface expression of

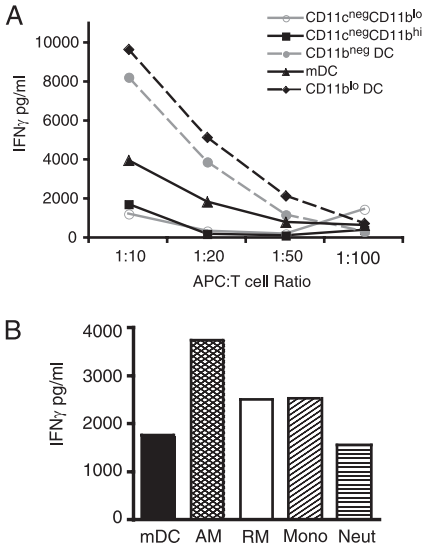

FIGURE 7. Ag-specific CD4$^+$ T lymphocyte-stimulating capacity of CD11c/CD11b-defined cell subsets from lungs and mediastinal lymph nodes of Mtb-infected mice. *A*, Cells in each of the CD11c/CD11b-defined subsets in the mediastinal lymph node of mice infected 28 days earlier were sorted by FACS and combined with Mtb Ag85B-specific transgenic CD4$^+$ T lymphocytes (P25 TCR-Tg) at the designated ratios in the presence of antigenic peptide. Three days later supernatants were assayed for the presence of IFN-γ to assess T cell activation. mDC, myeloid DC. *B*, Cells in each of the CD11c/CD11b-defined subsets from the lungs of mice infected for 28 days were sorted by FACS and combined with P25 TCR-Tg CD4 T cells at 1:10 APCs to T cells. After a three-day incubation, supernatants were assayed for IFN-γ. Graphs are representative of five independent experiments with each tissue. mDC, Myeloid DC; RM, recruited interstitial macrophage; AM, alveolar macrophage; Mono, monocyte; Neut, neutrophil.

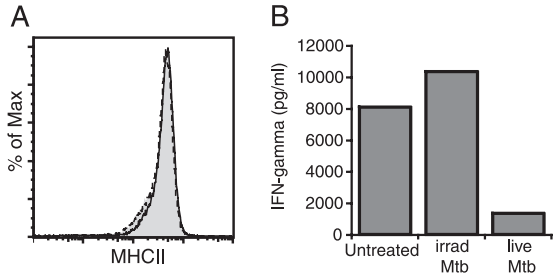

FIGURE 8. Inhibition of Ag presentation by Mtb in vitro. *A*, Histogram of surface expression of MHC class II on the clone of CIITA-RAW cells used for Ag-presentation experiments. Shaded area, Untreated CIITA-RAW cells; dashed line, CIITA-RAW cells exposed to gamma-irradiated Mtb; dotted line, CIITA-RAW cells infected with live Mtb. *B*, CIITA-RAW cells were exposed to gamma-irradiated (irrad) or live Mtb or medium alone and assayed for their ability to present OVA peptide (325–339) to Th1-polarized DO11.10 T cells, assayed as the production of IFN-γ after 48 h. The results shown are representative of four independent experiments.

MHC class II or a reduction in the surface expression of CD80 or CD86. Inhibition of Ag presentation by the CIITA-RAW cells required live Mtb, as no effect was observed when the cells were treated with gamma-irradiated Mtb.

Inefficient CD4$^+$ T cell stimulation is accompanied by the accumulation of intracellular bacteria in lung DCs and recruited macrophages

CD4$^+$ T cells provide protection against progressive growth of Mtb by secreting TNF and IFN-γ and by incompletely characterized cell contact-dependent mechanisms (26–28). The observation that Mtb-infected recruited interstitial macrophages and myeloid DCs were poorly recognized by Mtb-specific CD4$^+$ T cells suggests that these cells would be permissive for intracellular growth of Mtb in vivo. To test this hypothesis, we counted the number of bacteria per cell after sorting GFP$^+$ myeloid DCs and recruited macrophages from the lungs (Fig. 9). Accurate enumeration of the number of bacteria per cell was only possible at low cellular bacterial densities, so we used a conservative cutoff and scored all cells with five or more bacteria as having five bacteria per cell. Despite this conservative cutoff, we found that lung DCs contained 3.76 ± 0.05 bacteria per cell, whereas recruited macrophages contained 4.13 ± 0.05 bacteria/cell ($p = 0.0001$, by Mann-Whitney U test). Moreover, while 32% of infected lung DCs contained at least five bacteria per cell, nearly twice as many infected recruited macrophages (59%) contained at least five bacteria per cell and many of the macrophages were densely packed with bacteria, whereas few densely infected DCs were found (Fig. 9). These findings indicate that multiple subsets of APCs are permissive for the growth of Mtb in vivo and that cells that stimulate Ag-specific CD4$^+$ T cells poorly contain more bacteria per cell.

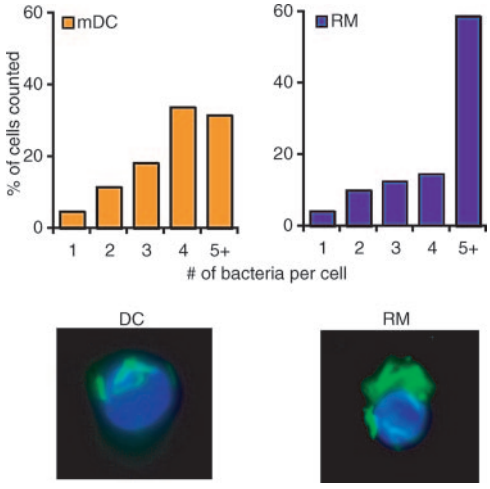

FIGURE 9. Frequency distribution of the number of Mtb-GFP per cell in recruited macrophages (RM)and DCs isolated from lungs (day 21 postinfection). GFP$^+$ recruited macrophages and DCs were sorted by FACS and nuclei were visualized with 4′,6′-diamidino-2-phenylindole. Approximately 450 cells of each type were examined by fluorescent microscopy and the number of bacteria in each cell was assessed visually, with all cells that contained at least five bacteria per cell counted as "5+." Micrographs show representative cells from the DC 5+ bacteria per cell group and the recruited macrophage 5+ bacteria per cell group. mDC, myeloid DC.

Discussion

The studies reported here reveal several major findings regarding the early stages of infection and the adaptive immune response after aerosol infection with Mtb. First, they demonstrate that Mtb infects cells of diverse phenotypes, that the predominant infected cell populations change with time, and that myeloid DCs are one of the major cell populations that are infected with Mtb in the lungs and lymph nodes. Second, we found that the population of Mtb-infected cells in the lung-draining lymph node is much less diverse than that in the lungs; up to 80% of the bacteria in the lymph node are found in myeloid DCs. Moreover, we found evidence that the bacteria in the lung-draining lymph node are transported there from the lungs by a CCL19/21-dependent mechanism and that the transport of bacteria to the lymph node is a transient phenomenon. Third, we found that the lymph node cell subsets that are most efficacious in presenting an Mtb peptide Ag to CD4$^+$ T lymphocytes are not infected with the bacteria and are not represented in the lungs of infected mice. Finally, we found that the cell populations that are infected with Mtb at high frequency are relatively ineffective at stimulating Ag-specific CD4$^+$ T cells, and we have obtained evidence that live Mtb can inhibit MHC class II Ag presentation without a decrease in the surface expression of MHC class II.

Since 1925, mononuclear phagocytes have been known to be resident cells for Mtb in vivo (11). Until recently, Mtb has been thought to reside exclusively in macrophages, although recent studies have detected bacteria in DCs in tissues of mice and humans (12, 13, 29). The sensitive and specific flow cytometry assay we have developed has allowed us to detect and characterize cells infected with GFP-expressing Mtb and to find that the cell populations that contain Mtb during the initial 4 wk of infection are highly dynamic and that DCs, not macrophages, are the quantitatively predominant subset of the infected cells in the lungs after the first 2 wk of infection. In the studies reported here, lung DCs were identified by their high-level expression of both CD11c and CD11b as previously described (15–17). In addition, we found that this cell subset in the lungs exhibits other characteristics of DCs, including IFN-γ-independent expression of high levels of surface MHC class II and high levels of the costimulatory molecules CD80 and CD86. This same subset of cells in the lungs has been found by other investigators to exhibit additional properties of DCs, including characteristic morphology in situ (17), the ability to migrate from the lungs to the mediastinal lymph node (16, 30), and the ability to prime naive T cells (16, 17). Moreover, we found that a large fraction of the infected cells in the lungs express the DC marker DEC-205 as determined by immunohistochemistry. Although our findings indicate that lung DCs are a major cell subset

infected with Mtb, they do not establish whether the infected cells exhibited a DC phenotype before infection or whether a subset of macrophages undergoes a transition to a DC phenotype in response to Mtb infection.

The number of DCs and recruited macrophages in the lungs increases progressively during the first 4 wk of infection, at least in part due to CCR2-dependent signaling (31–33), and upon arrival in the lungs the DCs and recruited macrophages become infected and markedly outnumber the initially infected alveolar macrophages, which do not change in total number or the number of infected cells after the first 2 wk of infection. After the 3rd wk of infection, newly recruited DCs and macrophages together account for 80–90% of the infected cells in the lungs, and afterward the distribution of the bacteria in these cells remains stable. Between days 14 and 19 postinfection, concurrent with DC recruitment and infection in the lungs, DCs mature as assessed by expression of surface MHC class II and the costimulatory molecules CD80 and CD86. Within this same interval, infected DCs transport live Mtb from the lungs to the lung-draining mediastinal lymph node, which indicates that at least a subset of infected lung DCs express CCR7, CCR8, and/or other chemokine receptors required for migration, at least in the first 14–17 days of infection.

Within the lung-draining mediastinal lymph node, all of the subsets of cells defined by the expression of CD11b and CD11c increased in number by day 19 of infection, and all of them stayed persistently increased in number compared with that in uninfected mice for at least the first four weeks of infection. Of the lymph node cells that contained Mtb, up to 80% are $CD11c^{high}CD11b^{high}$ myeloid DCs, which implies that only this subset of cells, and neither of the macrophage subsets, is capable of migrating from the lungs to the lymph node, consistent with the results observed after the administration of fluorescent latex particles (16) or infection with an influenza virus (30). The number of Mtb-infected DCs in the lymph node reached a peak on day 21 after infection, when the number of DCs containing bacteria in the lungs also reached its maximum level. On day 21, the number of Mtb-infected myeloid DCs in the lymph node was ~10% of the number in the lungs, which suggests that during the initial weeks of infection a high proportion of the DCs in the lungs that become infected migrate from the lungs to the local lymph node. Unlike the pattern seen in the lungs, the number of infected myeloid DCs in the lymph node decreases markedly after day 21, so that by day 28 the number of infected cells in the lymph node is only 2% of that in the lungs. One potential explanation for this finding is that infected DCs stop migrating from the lungs to the lymph node, as has been observed for lung DCs after infection with an influenza virus (30). However, this is not likely to be the sole explanation, because the total number of myeloid DCs in the lymph node remains stable from days 19–28. An additional possibility is that total DC migration from the lungs does not cease but that migration of Mtb-infected DC is selectively arrested after days 17–21. Further studies will be required to determine whether selective differences in the migration of Mtb-infected and uninfected lung DCs occurs after an initial wave of migration of infected lung DCs. The finding that DC migration from the lungs to the lymph node is temporally restricted despite chronic infection implies that Mtb Ags that are only expressed during the later stages of infection may not be efficiently presented to naive T lymphocytes.

Because myeloid DCs are the predominant population of cells that contain Mtb in the mediastinal lymph node, we expected that they would also exhibit the highest capacity for Ag presentation to Mtb-specific $CD4^+$ T lymphocytes. Instead, the $CD4^+$ T cell stimulating capacity of myeloid DCs from the mediastinal lymph node was exceeded by that of two alternative populations of lymph node DCs that expressed low or negligible levels of CD11b. Because neither of these cell populations is infected at high frequency in vivo and because neither is found in the lungs, our results suggest that while myeloid DCs transport live Mtb from the lungs to the lymph node, the priming of naive Mtb-specific $CD4^+$ T lymphocytes may be accomplished by resident lymph node DCs as has been reported during the early immune response to *Leishmania major* after intradermal infection (34). Further studies will be necessary to determine the precise mechanism(s) of the presentation of Mtb Ags to naive $CD4^+$ T lymphocytes, including the quantitative roles of Ag produced by bacteria in the lungs or in the lymph node and the quantitative contributions of Ags acquired by DCs from apoptotic macrophages.

When we examined the Ag presentation capacity of DCs and macrophages isolated from the lungs of infected mice, we found that they were less able to stimulate Mtb Ag85B-specific $CD4^+$ T lymphocytes than were lymph node cells. Myeloid DCs from the lungs stimulated Mtb-specific $CD4^+$ T cells to secrete approximately half the amount of IFN-γ observed when DCs from the lymph node were used despite comparable levels of expression of surface MHC class II, CD80, CD86, and CD40. These results indicate that the DCs found in the lungs are less efficacious APCs than those in the lymph node. One possible explanation is that Mtb-infected lung DCs undergo a defective maturation program that limits their capacity to migrate to lymph nodes as well as to present peptide Ags by the class II pathway. Indeed, Mtb has been reported to inhibit the maturation of human peripheral blood-derived DCs in vitro (35), but the results reported here are the first to demonstrate that this phenomenon also occurs in vivo.

To seek evidence that Mtb inhibits MHC class II Ag presentation in cells that do not require treatment with IFN-γ for class II expression, we constructed a macrophage cell line that constitutively expresses CIITA, which drives high levels of surface class II. Using those cells, we found that live, but not gamma-irradiated, Mtb inhibits class II Ag presentation to $CD4^+$ T lymphocytes despite abundant surface class II. This cell line should prove valuable for studies of the cellular basis of the inhibition of class II Ag presentation and for screening libraries of mutant Mtb to identify bacterial mechanisms of inhibiting Ag presentation.

In addition to the poorer Ag-presenting capacity of DCs from the lungs compared with that of DCs from the lymph node, recruited lung macrophages exhibited even lower efficacy in stimulating Mtb Ag85B-specific $CD4^+$ T lymphocytes. This was accompanied by a lower surface expression of MHC class II and in the presence of a lower frequency of expression of CD80 and CD86 in recruited macrophages compared with that in lung DCs. That this may have functional relevance is indicated by our finding that recruited macrophages contain significantly more bacteria per cell than do DCs in the lungs, although from these experiments it is not possible to determine whether the greater number of bacteria is the cause or the effect of poor Ag presentation and T cell stimulation.

In summary, we have found that Mtb infects phagocytes with diverse phenotypes in vivo and that myeloid DCs transport Mtb from the lungs to the local lymph node during the early, but not later, stages of infection. Moreover, we have found that DCs and recruited macrophages in the lungs are poor stimulators of Mtb Ag-specific $CD4^+$ T cells. Taken together, these results imply that vaccines that induce cellular immune responses to Mtb Ags may have limited efficacy if the responding memory and effector T lymphocytes cannot effectively recognize infected lung cells. In addition to ongoing vaccine development, efforts to develop strategies for overcoming immune evasion by Mtb need to be a high priority.

Acknowledgments

We thank the staff of the Gladstone Institute Flow Cytometry Core for assistance with flow cytometry optimization, the staff of the New York University Center for AIDS Research for assistance with cell sorting, and Wendy Peters, Ph.D., for assistance during early stages of this work.

Disclosures

The authors have no financial conflict of interest.

References

1. Mogues, T., M. E. Goodrich, L. Ryan, R. LaCourse, and R. J. North. 2001. The relative importance of T cell subsets in immunity and immunopathology of airborne *Mycobacterium tuberculosis* infection in mice. *J. Exp. Med.* 193: 271–280.
2. North, R. J., and Y. J. Jung. 2004. Immunity to tuberculosis. *Annu. Rev. Immunol.* 22: 599–623.
3. Sonnenberg, P., J. R. Glynn, K. Fielding, J. Murray, P. Godfrey-Faussett, and S. Shearer. 2005. How soon after infection with HIV does the risk of tuberculosis start to increase? A retrospective cohort study in South African gold miners. *J. Infect. Dis.* 191: 150–158.
4. Opie, E., and J. Aronson. 1927. Tubercle bacilli in latent tuberculous lesions and in lung tissue without tuberculous lesions. *Arch. Pathol. Lab. Med.* 4: 1–21.
5. Robertson, H. 1933. The persistence of tuberculous infections. *Am. J. Pathol.* 9: 711–719.
6. Wang, C. 1917. An experimental study of latent tuberculosis. *Lancet* 2: 417–419.
7. Perlman, D. C., W. M. el-Sadr, E. T. Nelson, J. P. Matts, E. E. Telzak, N. Salomon, K. Chirgwin, and R. Hafner. 1997. Variation of chest radiographic patterns in pulmonary tuberculosis by degree of human immunodeficiency virus-related immunosuppression: The Terry Beirn Community Programs for Clinical Research on AIDS (CPCRA), the AIDS Clinical Trials Group (ACTG). *Clin. Infect. Dis.* 25: 242–246.
8. Shafer, R. W., A. B. Bloch, C. Larkin, V. Vasudavan, S. Seligman, J. D. Dehovitz, G. DiFerdinando, R. Stoneburner, and G. Cauthen. 1996. Predictors of survival in HIV-infected tuberculosis patients. *AIDS* 10: 269–272.
9. Cooper, A. M., D. K. Dalton, T. A. Stewart, J. P. Griffin, D. G. Russell, and I. M. Orme. 1993. Disseminated tuberculosis in interferon γ gene-disrupted mice. *J. Exp. Med.* 178: 2243–2247.
10. Flynn, J. L., J. Chan, K. J. Triebold, D. K. Dalton, T. A. Stewart, and B. R. Bloom. 1993. An essential role for interferon γ in resistance to *Mycobacterium tuberculosis* infection. *J. Exp. Med.* 178: 2249–2254.
11. Cunningham, R. S., F. R. Sabin, S. Sugiyama, and J. A. Kindwali. 1925. The role of the monocyte in tuberculosis. *Bull. Johns Hopkins Hosp.* 37: 231.
12. Tailleux, L., O. Schwartz, J. L. Herrmann, E. Pivert, M. Jackson, A. Amara, L. Legres, D. Dreher, L. P. Nicod, J. C. Gluckman, et al. 2003. DC-SIGN is the major *Mycobacterium tuberculosis* receptor on human dendritic cells. *J. Exp. Med.* 197: 121–127.
13. Humphreys, I. R., G. R. Stewart, D. J. Turner, J. Patel, D. Karamanou, R. J. Snelgrove, and D. B. Young. 2006. A role for dendritic cells in the dissemination of mycobacterial infection. *Microbes Infect.* 8: 1339–1346.
14. Tian, T., J. Woodworth, M. Skold, and S. M. Behar. 2005. In vivo depletion of $CD11c^+$ cells delays the $CD4^+$ T cell response to *Mycobacterium tuberculosis* and exacerbates the outcome of infection. *J. Immunol.* 175: 3268–3272.
15. Gonzalez-Juarrero, M., T. S. Shim, A. Kipnis, A. P. Junqueira-Kipnis, and I. M. Orme. 2003. Dynamics of macrophage cell populations during murine pulmonary tuberculosis. *J. Immunol.* 171: 3128–3135.
16. Jakubzick, C., F. Tacke, J. Llodra, N. van Rooijen, and G. J. Randolph. 2006. Modulation of dendritic cell trafficking to and from the airways. *J. Immunol.* 176: 3578–3584.
17. Landsman, L., C. Varol, and S. Jung. 2007. Distinct differentiation potential of blood monocyte subsets in the lung. *J. Immunol.* 178: 2000–2007.
18. Henri, S., D. Vremec, A. Kamath, J. Waithman, S. Williams, C. Benoist, K. Burnham, S. Saeland, E. Handman, and K. Shortman. 2001. The dendritic cell populations of mouse lymph nodes. *J. Immunol.* 167: 741–748.
19. Vremec, D., and K. Shortman. 1997. Dendritic cell subtypes in mouse lymphoid organs: cross-correlation of surface markers, changes with incubation, and differences among thymus, spleen, and lymph nodes. *J. Immunol.* 159: 565–573.
20. Medeiros, M. A., O. A. Dellagostin, G. R. Armoa, W. M. Degrave, L. De Mendonca-Lima, M. Q. Lopes, J. F. Costa, J. McFadden, and D. McIntosh. 2002. Comparative evaluation of *Mycobacterium vaccae* as a surrogate cloning host for use in the study of mycobacterial genetics. *Microbiology* 148: 1999–2009.
21. Tamura, T., H. Ariga, T. Kinashi, S. Uehara, T. Kikuchi, M. Nakada, T. Tokunaga, W. Xu, A. Kariyone, T. Saito, et al. 2004. The role of antigenic peptide in $CD4^+$ T helper phenotype development in a T cell receptor transgenic model. *Int. Immunol.* 16: 1691–1699.
22. Nakano, H., and M. D. Gunn. 2001. Gene duplications at the chemokine locus on mouse chromosome 4: multiple strain-specific haplotypes and the deletion of secondary lymphoid-organ chemokine and EBI-1 ligand chemokine genes in the plt mutation. *J. Immunol.* 166: 361–369.
23. Buettner, M., C. Meinken, M. Bastian, R. Bhat, E. Stossel, G. Faller, G. Cianciolo, J. Ficker, M. Wagner, M. Rollinghoff, and S. Stenger. 2005. Inverse correlation of maturity and antibacterial activity in human dendritic cells. *J. Immunol.* 174: 4203–4209.
24. Hertz, C. J., S. M. Kiertscher, P. J. Godowski, D. A. Bouis, M. V. Norgard, M. D. Roth, and R. L. Modlin. 2001. Microbial lipopeptides stimulate dendritic cell maturation via Toll-like receptor 2. *J. Immunol.* 166: 2444–2450.
25. Somoskovi, A., G. Zissel, M. W. Ziegenhagen, M. Schlaak, and J. Muller-Quernheim. 2000. Accessory function and costimulatory molecule expression of alveolar macrophages in patients with pulmonary tuberculosis. *Immunobiology* 201: 450–460.
26. Bonecini-Almeida, M. G., S. Chitale, I. Boutsikakis, J. Geng, H. Doo, S. He, and J. L. Ho. 1998. Induction of in vitro human macrophage anti-*Mycobacterium tuberculosis* activity: requirement for IFN-γ and primed lymphocytes. *J. Immunol.* 160: 4490–4499.
27. Cowley, S. C., and K. L. Elkins. 2003. $CD4^+$ T cells mediate IFN-γ-independent control of *Mycobacterium tuberculosis* infection both in vitro and in vivo. *J. Immunol.* 171: 4689–4699.
28. Silver, R. F., Q. Li, W. H. Boom, and J. J. Ellner. 1998. Lymphocyte-dependent inhibition of growth of virulent Mycobacterium tuberculosis H37Rv within human monocytes: requirement for $CD4^+$ T cells in purified protein derivative-positive, but not in purified protein derivative-negative subjects. *J. Immunol.* 160: 2408–2417.
29. Jiao, X., R. Lo-Man, P. Guermonprez, L. Fiette, E. Deriaud, S. Burgaud, B. Gicquel, N. Winter, and C. Leclerc. 2002. Dendritic cells are host cells for mycobacteria in vivo that trigger innate and acquired immunity. *J. Immunol.* 168: 1294–1301.
30. Legge, K. L., and T. J. Braciale. 2003. Accelerated migration of respiratory dendritic cells to the regional lymph nodes is limited to the early phase of pulmonary infection. *Immunity* 18: 265–277.
31. Peters, W., J. G. Cyster, M. Mack, D. Schlondorff, A. J. Wolf, J. D. Ernst, and I. F. Charo. 2004. CCR2-dependent trafficking of F4/80dim macrophages and CD11cdim/intermediate dendritic cells is crucial for T cell recruitment to lungs infected with *Mycobacterium tuberculosis*. *J. Immunol.* 172: 7647–7653.
32. Peters, W., H. M. Scott, H. F. Chambers, J. L. Flynn, I. F. Charo, and J. D. Ernst. 2001. Chemokine receptor 2 serves an early and essential role in resistance to *Mycobacterium tuberculosis*. *Proc. Natl. Acad. Sci. USA* 98: 7958–7963.
33. Scott, H. M., and J. L. Flynn. 2002. *Mycobacterium tuberculosis* in chemokine receptor 2-deficient mice: influence of dose on disease progression. *Infect. Immun.* 70: 5946–5954.
34. Iezzi, G., A. Frohlich, B. Ernst, F. Ampenberger, S. Saeland, N. Glaichenhaus, and M. Kopf. 2006. Lymph node resident rather than skin-derived dendritic cells initiate specific T cell responses after *Leishmania major* infection. *J. Immunol.* 177: 1250–1256.
35. Hanekom, W. A., M. Mendillo, C. Manca, P. A. Haslett, M. R. Siddiqui, C. Barry, III, and G. Kaplan. 2003. *Mycobacterium tuberculosis* inhibits maturation of human monocyte-derived dendritic cells in vitro. *J. Infect. Dis.* 188: 257–266.